# 8

# Comparison between model and experimental results obtained by imaging laser absorption spectroscopy

**Abstract.**
The effect of the competition between convection and diffusion on the distribution of metal-halide additives in a high pressure mercury lamp has been examined by placing COST reference lamps with mercury fillings of 5 mg and 10 mg in a centrifuge. By subjecting them to different accelerational conditions the convection speed of the mercury buffer gas is affected. The resulting distribution of the additives, in this case dysprosium iodide, has been studied by numerical simulations and measurements of the density of dysprosium atoms in the ground state using imaging laser absorption spectroscopy. The competition between axial convection and radial diffusion determines the degree of axial segregation of the dysprosium additives.

Sections 8.1–8.8 have been adapted from [M.L. Beks, A.J. Flikweert, T. Nimalasuriya, W.W. Stoffels and J.J.A.M. van der Mullen, *Competition between convection and diffusion in a metal halide lamp, investigated by numerical simulations and imaging laser absorption spectroscopy*, J. Phys. D: Appl. Phys. **41** (2008) 144025].

Section 8.9 has been adapted from [A.J. Flikweert, M.L. Beks, T. Nimalasuriya, G.M.W. Kroesen, J.J.A.M. van der Mullen and W.W. Stoffels, *2-D Images of the Metal-Halide Lamp Obtained by Experiment and Model*, IEEE Trans. on Plasma Science **36** (2008) 1174–1175].

## 8.1 Introduction

High intensity discharge (HID) lamps are very efficient light sources in widespread use today. They are, amongst others, in use as automotive headlight lamps and to light shops, roads, sports stadiums and large indoor spaces. HID lamps containing a mixture of mercury and metal iodide salts are known as metal-halide (MH) lamps. These devices combine high luminous output with excellent colour rendering. In earlier publications [86, 87] we examined the distribution of additives through numerical modelling. In this publication we will expand the earlier model to allow the simulation of lamps containing metals such as dysprosium. This also allows us to compare the results with experiments [50]. Additionally, we have simulated the lamp under various accelerational conditions to compare with experiments done in a centrifuge (see chapter 4) [37, 38, 51, 52].

One well-known fact [25, 28, 88] is that, when operated vertically, the metal halides in the lamp tend to demix; the concentration of metal halides in the gas phase is much greater at the bottom of the lamp. This effect is not present under all conditions, and some lamp designs are more severely affected than others. The demixing can be observed directly from the light output; a demixed lamp shows a bluish green mercury discharge at the top of the lamp and a much brighter and whiter discharge from the additives at the bottom of the lamp [23]. Demixing, or axial segregation as it is also called, has a negative impact on the efficacy of the lamp. It is currently avoided by using lamp designs with very short or very long aspect ratios. Gaining more insight into the process of demixing could possibly allow a broader range of lamp designs with still better luminous efficacies.

## 8.2 Demixing

Demixing is caused by a competition between convection and diffusion [28]. Under operating conditions the mercury in the lamp is completely vaporized providing a buffer gas with a pressure of several bar. The additives do not completely vaporize and form a salt pool at the bottom of the lamp. Typical vapour pressures of the additives are in the range of several millibar. The additive molecules diffuse inwards from the wall into the centre of the plasma where they dissociate to form free atoms. These are partially ionized. The atoms diffuse outwards back toward the wall more readily than the molecules diffuse inward. Under (quasi) steady state operation and in the absence of convection the net flux of elements is zero.

Let us assume, for the purpose of this discussion, that the diffusion is given by Fick's law.[1] The flux of species $i$ $\vec{\Gamma}_i$ is then given by

$$\vec{\Gamma}_i = -D_i \nabla p_i, \tag{8.1}$$

[1]Note that, in general, the diffusion of species in the plasma does not obey Fick's law and the numerical model does not assume this as discussed in the following section.

with $D_i$ the diffusion coefficient and $p_i$ the partial pressure of species $i$. In the absence of convection, the flux of atoms towards the walls must equal the flux of molecules away from the walls multiplied with the stoichiometric coefficient. Substitution of this equality into equation (8.1) results in

$$R_{\mathrm{mol,element}} D_{\mathrm{mol}} \nabla p_{\mathrm{mol}} = -D_{\mathrm{atom}} \nabla p_{\mathrm{atom}}, \tag{8.2}$$

with $R_{\mathrm{mol,element}}$ the stoichiometric coefficient. Rearranging the above leads to

$$\nabla p_{\mathrm{atom}} = -\left(\frac{R D_{\mathrm{mol}}}{D_{\mathrm{atom}}}\right) \nabla p_{\mathrm{mol}}. \tag{8.3}$$

Since $D_{\mathrm{atom}} > D_{\mathrm{mol}}$ a larger gradient of the molecular partial pressure can be supported ($\nabla p_{\mathrm{atom}} < \nabla p_{\mathrm{mol}}$). Thus, radial segregation occurs, with more of the additive in the form of molecules near the walls than in the form of atoms in the centre of the discharge. The stoichiometric coefficient is also of importance, however, as each $DyI_3$ molecule transports three iodine atoms as it diffuses towards the wall. Thus the radial iodine segregation is limited.

The large temperature gradients in the lamp drive natural convection. The convection of the buffer gas drags the additives down along the walls and up again through the centre of the discharge. Because the atoms diffuse outwards more readily than the molecules diffuse inwards the additives stay at the bottom of the discharge. This effect is known as axial segregation.

When the convective and diffusive processes are in the same order of magnitude, the axial segregation of the metal additive is maximal. In the two limiting cases, when there is no convection or when there is extremely high convection no axial segregation is present. In [86] we presented a study that describes this convection-diffusion (CD) competition in full detail. For this we used a model that was constructed by means of the grand model platform PLASIMO [89]. This model gives a self-consistent calculation of the competition between convection, diffusion, the local thermodynamic equilibrium (LTE) chemistry, the electric field and the radiation transport. In [87] we improved the model by taking the shape of the electrode into account. This model with penetrating electrodes was run for a series of mercury pressures and it was found that the electrodes influence convection patterns in the lamp. Both [86] and [87] were based on MH lamps consisting of a mixture of Hg and NaI. To compare with experiments the authors have extended the model to work with dysprosium iodide. Results comparing with experiments under micro-gravity have been examined in [71].

Because the convection is induced by gravity, varying the accelerational conditions aids the understanding of the diffusive and convective processes inside the lamp. A centrifuge, which can go up to $10g$, was built for this purpose (chapter 4) [33, 37, 41, 43, 51, 52]. The MH lamp that is investigated in the centrifuge is a COST lamp [27]. It contains 4 mg $DyI_3$ as salt additive, which is partially evaporated when the lamp is burning. In the centrifuge setup, the ground state Dy density distribution is measured

by means of imaging laser absorption spectroscopy (ILAS) [37]. These experimental results are compared with the model.

## 8.3 Model description

We will give a short overview of the basic equations solved in the model. More details are presented in [71, 86, 87]. The model assumes LTE [90].

### 8.3.1 Energy balance

All modules come together in the energy balance to calculate the plasma temperature. The temperature, in turn, strongly influences the transport coefficients, composition, flow and radiation. The temperature is given by

$$\nabla \cdot (C_p \vec{u} T) - \nabla \cdot (K \nabla T) = P - Q_{rad}, \tag{8.4}$$

where $C_p$ is the heat capacity at constant pressure, $\vec{u}$ the bulk velocity, $K$ the thermal conductivity, $Q_{rad}$ the net radiated power and $P$ the Ohmic dissipation ($P = \sigma E^2$).

The term $Q_{rad}$ is the result of 2D ray-tracing. We solve the equation for the radiation intensity $I_\nu$ [91]

$$\frac{dI_\nu}{ds} = j_\nu - \kappa I_\nu, \tag{8.5}$$

with $j_\nu$ the local emission coefficient and $\kappa$ the local coefficient for absorption along rays passing through the discharge [87]. The net radiated power is given by [91]:

$$Q_{rad} = \int_\nu \left( 4\pi j_\nu - \int_{4\pi} \kappa I_\nu d\Omega \right) d\nu, \tag{8.6}$$

with $\nu$ the frequency. For the precise form of $Q_{rad}$ for a $DyI_3$–Hg mixture we refer to [91]. To form the boundary conditions the electrodes are assumed to have a surface temperature of 2900 K and the rest of the wall a temperature of 1200 K.

### 8.3.2 Bulk flow

The bulk flow follows from the Navier-Stokes equation:

$$\nabla \cdot (\rho \vec{u} \vec{u}) = -\nabla p + \nabla \cdot (\mu \nabla \vec{u}) + \rho \vec{a}_g, \tag{8.7}$$

with $p$ the pressure, $\vec{a}_g$ the local (gravitational) acceleration, $\mu$ the dynamic viscosity and $\rho$ the density of the plasma.

### Particle transport

Since we assume LTE, the particle densities may be described by the local temperature, pressure and elemental composition. A convenient quantity to describe the distribution of elements is the elemental pressure. It is defined as the pressure that contains all molecular, atomic and ionic contributions of a particular element. The elemental pressure $p_\alpha$ for the element $\alpha$ can be written as

$$p_\alpha = \sum_i R_{i\alpha} p_i, \tag{8.8}$$

with $p_i$ the partial pressure of the species $i$, and $R_{i\alpha}$ the stoichiometric coefficient [86]. We solve a conservation equation for the elemental pressure

$$\nabla \cdot \left( \frac{D_\alpha}{kT} \nabla p_\alpha + \frac{p_\alpha}{kT} \vec{c}_\alpha \right) = 0, \tag{8.9}$$

with an effective diffusion coefficient $D_\alpha$ [86]

$$D_\alpha = p_\alpha^{-1} \sum_i R_{i\alpha} D_i p_i \tag{8.10}$$

and a pseudo convective velocity $c_\alpha$ [86].

To fix the boundary conditions we assume the existence of a cold spot at the bottom corner of the lamp, where the elemental pressure is derived from the x-ray induced fluorescence measurements at $1g$ of the elemental density of Dy and I at the cold spot [50]. Everywhere else the flux through the wall is zero.

Direct measurements of the elemental pressure at the walls are not possible for the lamps in the centrifuge, therefore we assume a Dy elemental pressure at the wall of 517 Pa and an I elemental pressure of 4268 Pa. These vapour pressures were determined with x-ray induced fluorescence measurements at $1g$ [50]. These are assumed to give a good estimation of the vapour pressure at the walls and are used to fix the boundary conditions. Note that there is an excess of iodine in the cold spot. This excess occurs because dysprosium is absorbed by the walls of the lamp.

### Ohmic heating

The power to the plasma is supplied by Ohmic heating. We solve the Poisson equation in the form

$$\nabla \cdot (\sigma_{el} \nabla \Phi) = 0, \tag{8.11}$$

with $\Phi$ the potential. From the potential $\Phi$ we can derive the electric field $\vec{E} = -\nabla\Phi$ and the current density $\vec{J} = \sigma_{el}\vec{E} = -\sigma_{el}\nabla\Phi$. The following boundary conditions are employed:

1. There is no current through the walls, resulting in a homogeneous Neumann boundary condition ($(\partial\Phi/\partial n) = 0$).

2. One electrode is kept at zero potential, which leads to a Dirichlet condition $\Phi = 0$ at that electrode.

3. The potential of the other electrode is initially set at 100 V. This value is adjusted during the iteration process and determined by the fact that the power dissipated in the discharge equals 135 W. This is equivalent to the actual lamp power of 150 W of which 15 W is consumed by electrode losses and 135 W by ohmic dissipation of the discharge.

### The selection of cross-sections

In the basic equations, summarized in the previous section, important roles are played by various transport coefficients, such as the diffusion coefficients $D_i$, the thermal conductivity $K$ and the electrical conductivity $\sigma_{el}$. These transport properties are calculated from collision integrals that are based on differential cross-sections [92]. More information on the cross-sections used can be found in [71].

## 8.4 Competition between convection and diffusion

The competition between convection and diffusion drives axial segregation in the lamps. For a quantitative description we use the Peclet number, well known from the field of fluid dynamics [93, page 85] which describes the competition between convection and diffusion in a dimensionless number. In this chapter we define the Peclet number as the ratio of the typical axial convection and radial diffusion rates. In terms of the typical axial convection velocity $V_z$, the height of the lamp burner $H$, the radius of the burner $R$ and the effective elemental diffusion coefficient introduced earlier the Peclet number is defined as

$$Pe = \frac{R^2 V_z}{H D_\alpha}. \tag{8.12}$$

A high Peclet number ($Pe \gg 1$) corresponds to the situation where the additive does not have time to diffuse radially outwards towards the walls when transported up with the hot mercury atoms in the centre of the lamp. In this case axial segregation cannot occur. For low Peclet numbers ($Pe \ll 1$) the rate of diffusion towards the walls is much greater than the rate of convection, and axial segregation is also absent. Axial segregation is most pronounced at intermediate values ($Pe \approx 1$), as will be shown in the results.

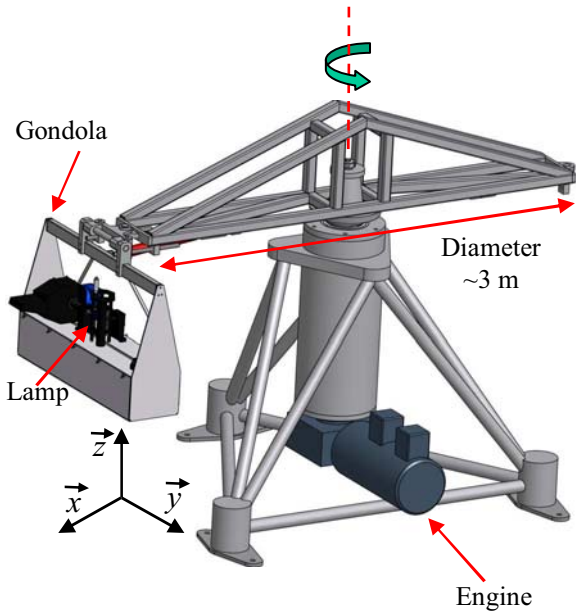


**Figure 8.1:** Schematic representation of the centrifuge. The coordinate system shown is that of the lamp in the gondola; this is a co-moving system such that $\vec{z}$ is always parallel to the lamp axis [37].

## 8.5 Experiment

A centrifuge was built as a tool to investigate MH lamps [27] under hyper-gravity conditions up to $10g$ and vary the convection speed in this way. In the following section the results will be compared with the results from the model.

### 8.5.1 Measurement technique

The experiment has been described in chapter 4 [37]; a summary will be given for clarity. The centrifuge shown in figure 8.1 consists of a pivot, an arm connected to the pivot and at the end of the arm a gondola that contains the lamp and diagnostic equipment. The total diameter at maximum swing-out of the gondola is close to 3 m. The total acceleration vector is always parallel to the lamp axis.

The measurement technique that is used in the centrifuge is ILAS. By using this technique, the 2D density distribution of the ground state Dy atom can be obtained. The principle is as follows. A laser beam is expanded so that it illuminates the full lamp burner. When the lamp is switched on, part of the laser light is absorbed by

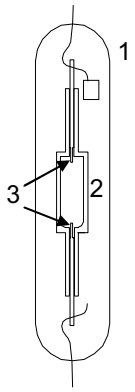


**Figure 8.2:** Schematic picture of the lamp, (1) outer bulb; (2) burner with height 20 mm and diameter 8 mm; (3) electrodes, distance between both electrodes ∼18 mm [27].

Dy atoms in the ground state. Behind the lamp, the light that is transmitted by the lamp burner is detected. By comparing the detected laser intensity with and without absorption, the line-of-sight ground state atomic dysprosium density is obtained for each position in the lamp burner.

### 8.5.2 The lamp

The investigated lamps are COST reference lamps (section 1.3.1) [27], see figure 8.2. The lamps are 20 mm in height (18 mm electrode distance) and 8 mm in diameter. They contain either 5 or 10 mg Hg. Furthermore they contain 4 mg $DyI_3$ as salt additive and 300 mbar $Ar/Kr^{85}$ as a starting gas. The input power is 148 W; the acceleration $a_z$ is varied from $1g$ to $10g$.

## 8.6 Results

The model was run for a set power $P_S$ of 135 W and compared with experimental results using a 148 W ballast. The difference of 13 W is an estimation of the electrode losses which are not accounted for in the model. Experiments were done with lamp fillings of 5 and 10 mg Hg. The model was run with lamp fillings ranging from 3 to 20 mg Hg. To fix the boundary conditions for the elemental pressure we assume the existence of a cold spot at the bottom corner of the lamp, where the elemental pressure is derived from the x-ray induced fluorescence measurements at $1g$ of the elemental density of Dy and I at the cold spot [50]. Everywhere else the flux through the wall is zero.

Direct measurements of the elemental pressure at the walls are not possible for the lamps in the centrifuge, therefore we assume a Dy elemental pressure at the wall of 517 Pa and an I elemental pressure of 4268 Pa. These vapour pressures were determined with x-ray induced fluorescence measurements at $1g$ [50]. These are assumed to give a good estimation of the vapour pressure at the walls and are used to fix the boundary conditions. Note that there is an excess of iodine in the cold spot. This excess occurs because dysprosium is absorbed by the walls of the lamp.

The density of dysprosium atoms was measured with the ILAS technique described in the previous section. The lamp underwent centripetal acceleration in the centrifuge from $1g$ to $10g$. The measurement technique yields the column density of dysprosium atoms in the ground state along the line of sight. The model yields many more results, of which only a minor part can be directly correlated with the experiment. We present some of the model results separately for further insight into the mechanisms behind what is observed experimentally.

The model solves differential equations for the total pressure, the velocity, the temperature, the electric potential and the elemental pressures. From these a number of derived quantities are obtained, notably the species densities and the radiation intensity. We will first present the elemental pressures at different lamp pressures and under different accelerational conditions.

### 8.6.1 Elemental pressure

The elemental dysprosium pressure at $1g$ and $2g$ with 10 mg of mercury given in figure 8.3(a) clearly shows both axial and radial segregation. The amount of dysprosium in the top of the lamp increases with increasing centripetal acceleration.

When one examines figure 8.3(a) carefully, local minima and maxima can be seen in the elemental dysprosium pressure. These are shown more clearly in the profiles for a total mercury content of 5 mg shown in figure 8.4. These local minima and maxima are not present if convection is switched off in the model, as is shown in figure 8.5. For more results comparing this model with micro-gravity experiments we refer to [71]. In figure 8.6 the axial convection speed is plotted. The axial speed is greater in the centre of the lamp than at the edges, due to the lower density and the smaller cross-sectional area in the centre. Consequently, the elemental dysprosium concentration in the centre rises as the acceleration increases. The radial position where the axial velocity crosses through zero does not show the same increase in elemental dysprosium. The result is that with the increase in convection more dysprosium enters the discharge and that the step like radial profile is disturbed.

### 8.6.2 Atomic dysprosium density

The experiment measures the column density of dysprosium atoms in the ground state. The model calculates the dysprosium atom density from the elemental pressure, total

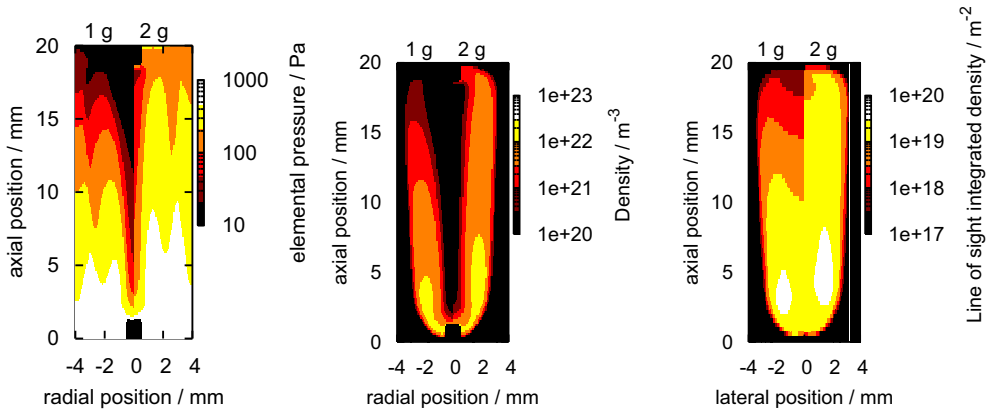


**Figure 8.3:** (a) Simulated elemental dysprosium pressure for a lamp with a 10 mg mercury filling at $1g$ (left) and $2g$ (right). (b) Simulated atomic dysprosium density for a lamp containing 10 mg of mercury at $1g$ and $2g$ simulated accelerational conditions. The $1g$ result is shown mirrored (negative radial positions) and the $2g$ result is shown on the right half of the graph. (c) Simulated column densities of dysprosium atoms for a lamp containing 10 mg of mercury at $1g$ and $2g$ simulated accelerational conditions. As in the previous graphs, the $1g$ results are shown mirrored with negative lateral positions.

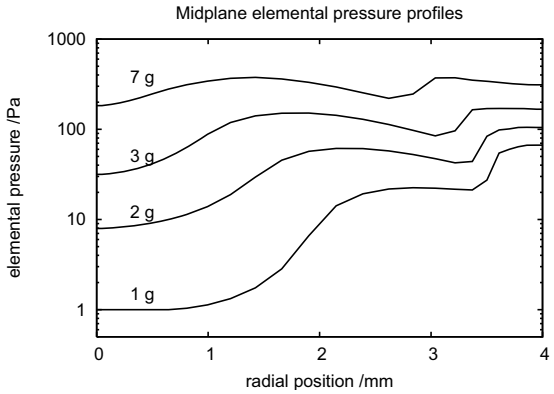


**Figure 8.4:** Simulated midplane elemental dysprosium pressure profiles for accelerational conditions ranging from $1g$ to $7g$ for a lamp with 5 mg of mercury filling. At low convection speeds the radial profiles have a shape comparable with the micro-gravity situation.

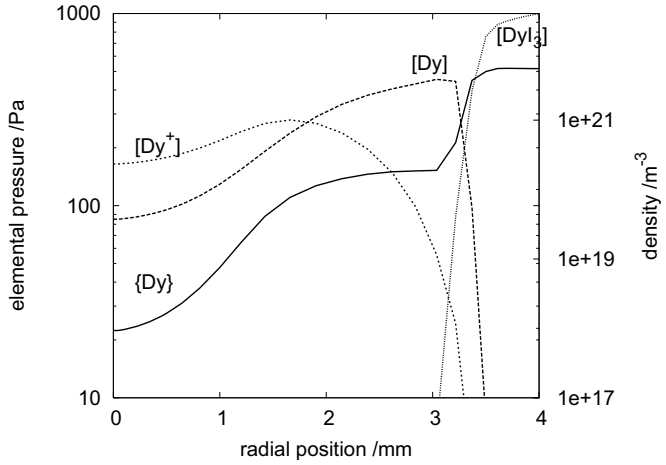


**Figure 8.5:** Simulated elemental dysprosium pressure ($Dy$ in the figure) with convection switched off (corresponding to micro-gravity). The discharge shows no axial segregation in this case. For comparison, the densities of the dysprosium ions, atoms and $DyI_3$ molecules are plotted (denoted with square brackets).

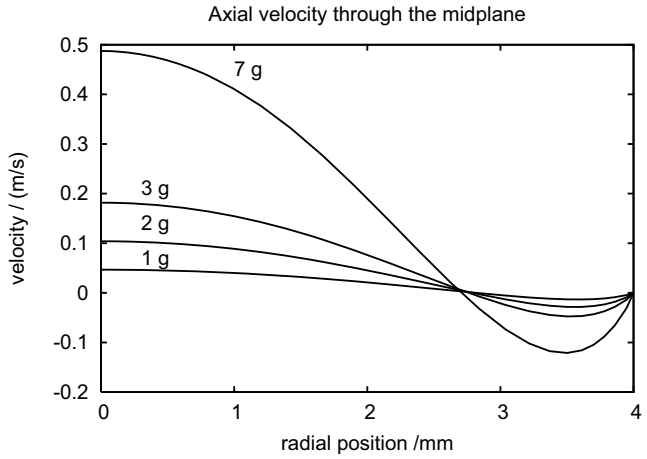


**Figure 8.6:** Simulated axial velocity through the midplane for accelerational conditions ranging from $1g$ to $7g$ in a lamp with 5 mg of mercury filling.

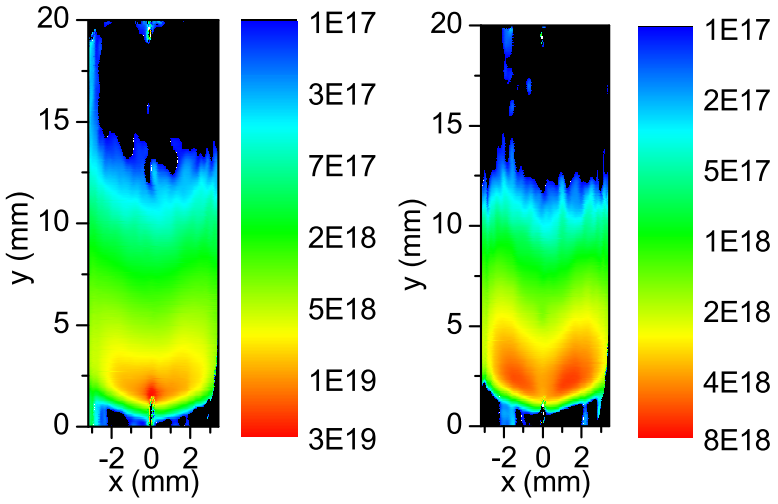


(a) $1g$ (b) $2g$

**Figure 8.7:** Experimental results for the ground state column densities of dysprosium atoms at (a) $1g$ and (b) $2g$ for a lamp containing 10 mg of mercury. Note that negative and positive lateral positions correspond to the left and the right side of the lamp, respectively.

pressure and temperature. An example of the calculated dysprosium density is shown in figure 8.3(b). As is evident in this figure, the dysprosium atom density decreases towards the top of the lamp. Increasing the convection speed by increasing the acceleration causes better mixing.

To compare with the experiments column densities have been calculated. These are shown in figure 8.3(c). For comparison, figure 8.7 shows the measured column densities of dysprosium atoms in the ground state. A qualitative comparison of these graphs shows a number of features present in both model and experiment. Most notable are the heart-shaped regions near the bottom of the lamp, where the dysprosium atoms are concentrated. Under higher accelerational conditions these regions move up slightly and become more elongated; this feature is present in both the model and the experiment.

For a more quantitative comparison, cross-sections of the results from both the model and the experiment at an axial position of 5 mm from the bottom of the lamp are shown in figure 8.8. As before, the results are for a lamp containing 10 mg of mercury under $1g$ and $2g$ acceleration in the centrifuge. The position of the maximum atom density in the simulations corresponds well to the maximum absorption in the experiment. The absolute values, however, do not agree. Figure 8.9 compares the measured atomic ground state density with the simulated atomic densities along the

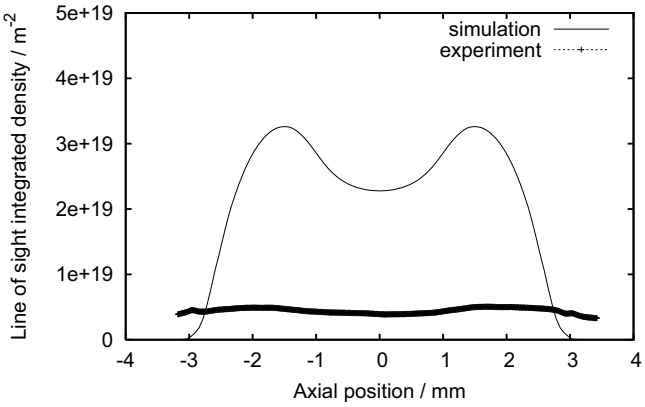


(a) $1g$

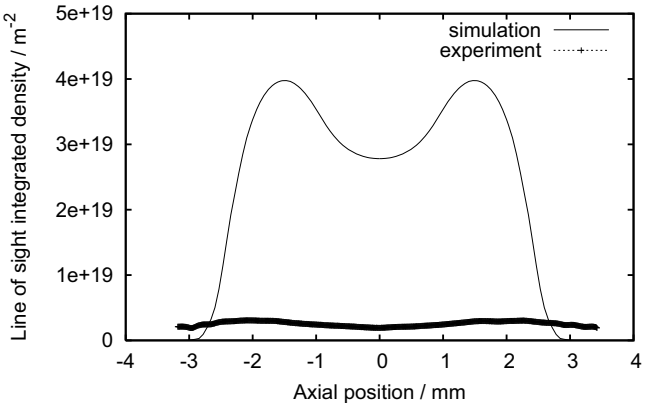


(b) $2g$

**Figure 8.8:** Experimental results for the ground state column densities of dysprosium atoms at (a) $1g$ and (b) $2g$ for a lamp containing 10 mg of mercury compared with the simulations. Results shown are at an axial position of 5 mm from the bottom of the lamp.

axis, and 2 mm off-axis. These results show good qualitative agreement between the simulation and the experiment. In particular, the position of the maximum density shows good agreement. The densities in the simulation are generally much larger. A possible reason might be the assumed cold spot vapour pressure. The cold spot vapour pressure depends exponentially on the temperature, as shown in figure 8.10. During the lifetime of the lamp, however, dysprosium migrates into the quartz walls. The individual lamps also differ. A change in the temperature of just 10 K leads to a 30 % increase in the vapour pressure just above the cold spot.

## 8.7 Cold spot vapour pressure

To further investigate the dependence on the cold spot vapour pressure, the model was rerun with dysprosium vapour pressures of 100–400 Pa in steps of 50 Pa. This study revealed that a dysprosium vapour pressure of 150 Pa, corresponding with a temperature of 1100 K, gave the closest match with experimental results. Figure 8.11 shows the ground state line-of-sight integrated densities of the dysprosium atoms at 5 mm from the bottom electrode for vapour pressures between 100 and 250 Pa compared with experimental results. The results with the 150 Pa vapour pressure also match well at other distances from the electrodes, as shown in figure 8.12, which compares lateral ground state densities as predicted by the model with a cold spot vapour pressure of 150 Pa with experiments along a line 2 mm off-axis. A line 2 mm off-axis is chosen as it offers the largest signal, and hence the best signal-to-noise ratio.

Varying the cold spot vapour pressure also allows us to study the effect of the radiation emitted by the additive. In the limit that the cold spot vapour pressure of dysprosium approaches zero the lamp becomes a pure mercury lamp again. Figure 8.13 shows the resulting temperature profiles in the midplane between the electrodes. From this figure it becomes evident that increasing the dysprosium elemental vapour pressure increases the contraction of the arc. This finding is in line with earlier findings and is due to the radiation emitted by dysprosium. By adding more dysprosium to the discharge radiative cooling is increased. The greatest concentration of emitting species is found just off-centre. The radiation emitted by dysprosium is optically open and not reabsorbed near the walls. Thus the radiation cools down the plasma on the flanks. To still allow sufficient current to pass through the plasma the centre has to become hotter. Hence, the observed contraction of the arc.

The hotter centre also results in increased convection, as is shown in figure 8.14. This is simply due to the larger temperature difference. The larger temperature difference translates directly into larger density gradients, which drive the convective flow.

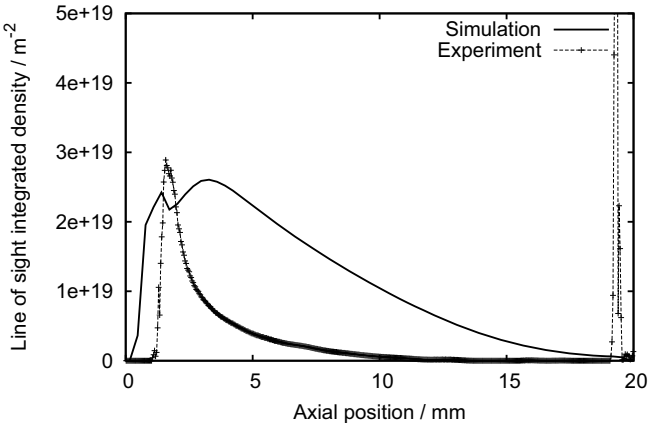


(a) Along the axis

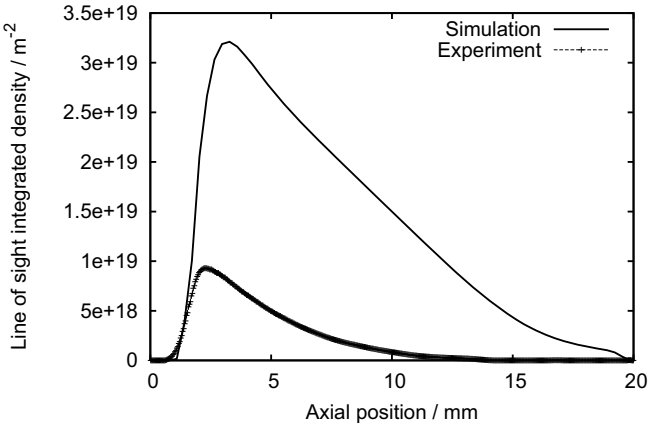


(b) 2 mm off-axis

**Figure 8.9:** Experimental results for the ground state column densities of dysprosium atoms at $1g$ for a lamp containing 10 mg of mercury compared with the simulations. Results shown are (a) along the axis and (b) 2 mm off-axis.

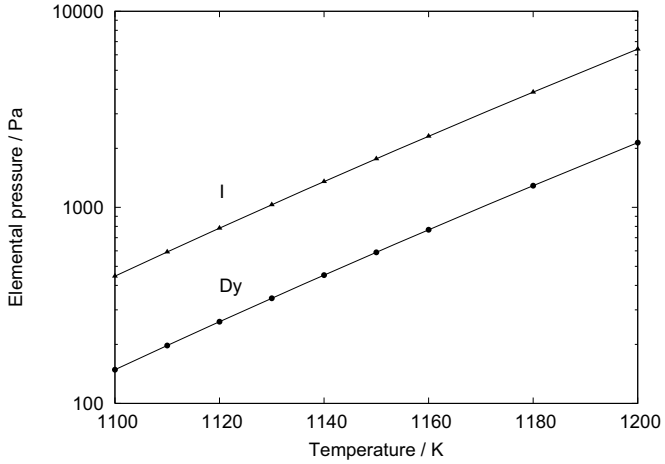


**Figure 8.10:** Elemental vapour pressure of dysprosium and iodide, as calculated by Gibbs minimization for temperatures between 1100 K and 1200 K.

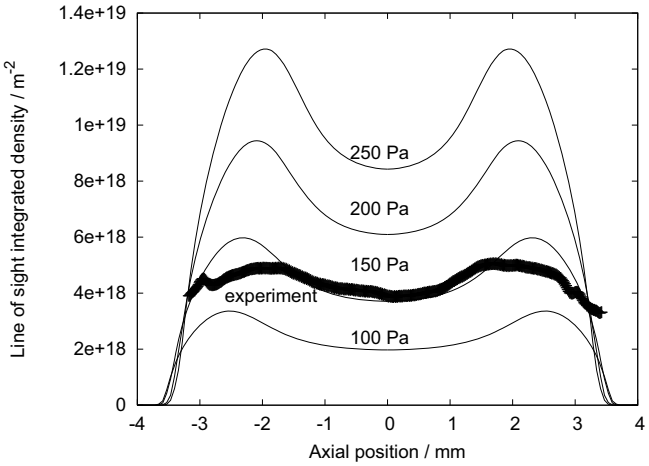


**Figure 8.11:** Experimental results for the ground state column densities of dysprosium atoms at $1g$ for a lamp containing 10 mg of mercury compared with the simulations at vapour pressures from 100 to 250 Pa. Results shown are at an axial position of 5 mm from the bottom of the lamp.

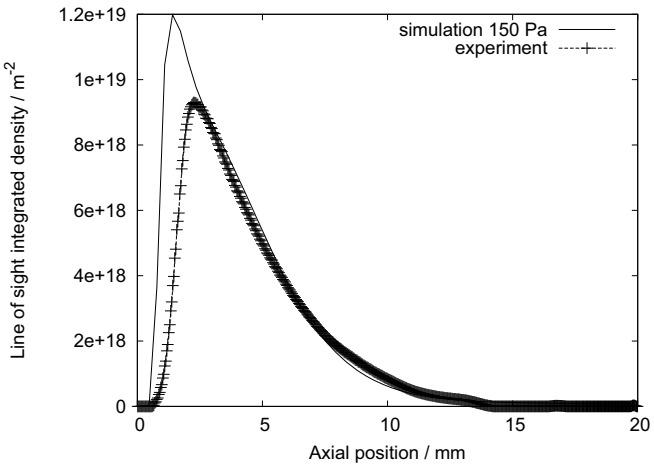


**Figure 8.12:** Experimental results for the ground state column densities of dysprosium atoms at $1g$ for a lamp containing 10 mg of mercury compared with the simulations at a vapour pressure of 150 Pa.

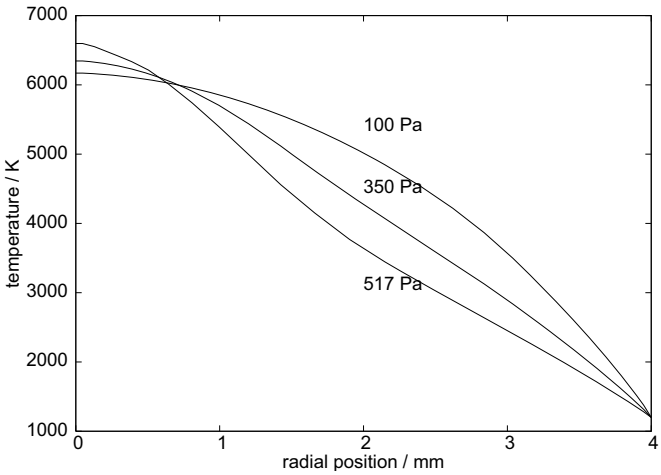


**Figure 8.13:** Midplane temperature profiles for three different cold spot vapour pressures: 517, 350 and 150 Pa. Adding more dysprosium clearly increases the contraction of the arc.

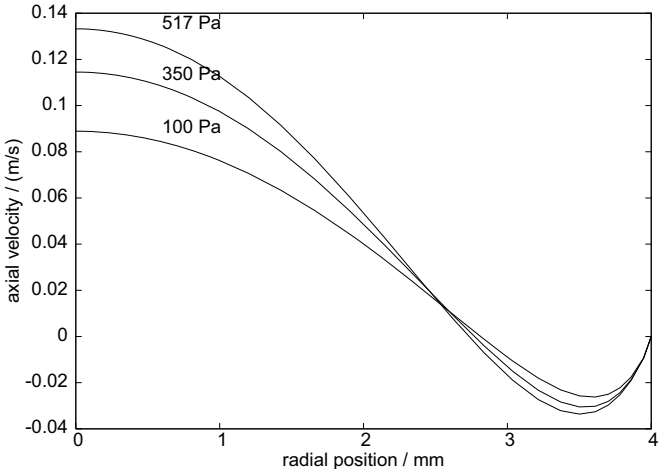


**Figure 8.14:** Midplane axial velocity profiles for three different cold spot vapour pressures: 517, 350 and 150 Pa. Adding more dysprosium increases the contraction of the arc and thereby increases the axial velocity through the midplane.

### 8.7.1 Demixing

We studied the demixing by defining the average segregation depth $\tau_\alpha$ of element $\alpha$ as

$$\tau = \frac{1}{V}\int_V \tau_H \mathrm{d}V, \tag{8.13}$$

with $\tau_H$ given by

$$\tau_H = \frac{H}{p_\alpha}\left(\frac{\partial p_\alpha}{\partial z}\right). \tag{8.14}$$

If $\tau$ is much smaller than unity the element is homogeneously distributed. Axial demixing occurs if $\tau$ is greater than unity.

To compare results with different lamp fillings we examine the segregation as a function of the Peclet number as defined in equation (8.12) (figure 8.15). We use the velocity on the axis halfway between the electrodes. The elemental diffusion coefficient is taken from the same spot. The model was run with a number of different pressures and simulated accelerational conditions. If we plot $\tau$ as a function of Peclet number a single curve emerges along which all results lie. The maximum point on this curve lies at $Pe = 1$.

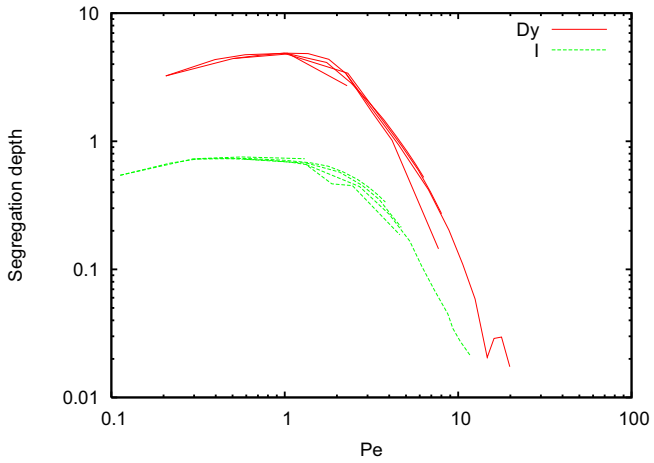


**Figure 8.15:** Segregation depth as a function of the Peclet number as defined by equation (8.12) obtained from the model. Lamp fillings between 3 and 20 mg and accelerational conditions between $1g$ and $10g$ are shown. Each lamp filling leads to a line in the figure. Note that $\tau$ has a maximum at $Pe = 1$. Iodine shows much less demixing than dysprosium.

## 8.8 Conclusions

A MH lamp with the COST geometry has been placed in a centrifuge to study the effect of the competition between convection and diffusion on the distribution of additives in the lamp. Using the plasma modelling platform PLASIMO, we have simulated the same lamp under different accelerational conditions. The density of dysprosium atoms in the ground state has been measured using the ILAS technique for different lamp fillings and accelerational conditions. These ground state densities show good qualitative agreement with the dysprosium atom densities predicted by the model.

The quantitative agreement between the model and experiments is not so good. One possible reason is the cold spot vapour pressure of the elements. This cold spot vapour pressure depends exponentially on the cold spot temperature. Increasing the temperature by 10 K is enough to raise the vapour pressure by 30%. Using a vapour pressure of 150 Pa rather than the value of 517 Pa measured by x-ray fluorescence (XRF) by Nimalasuriya *et al* [50] on similar lamps yields a better quantitative match between model and experiment.

The study with different vapour pressures also gives insight into the effects of the radiation emitted by the dysprosium additives. Increasing the partial pressure of dysprosium atoms and ions increases the radiation emitted by these species. Most of this radiation is emitted just off-centre from the axis. The radiative cooling by dyspro-

sium causes the arc to contract. Increasing the amount of dysprosium in the discharge increases arc contraction.

The competition between convection and diffusion can be understood quantitatively by introducing a Peclet number defined as the ratio between the rate of radial diffusion and axial convection. A Peclet number of unity leads to the greatest axial segregation. Increasing the convection speed by increasing the acceleration changes the radial profiles from a step-like profile to a more erratic profile with local minima and maxima. Obtaining a homogeneous distribution of additives in the lamp can be achieved by designing a lamp such that the Peclet number is much greater or much smaller than unity.

## Acknowledgements

The authors are grateful to Senter-Novem (project EDI 03146), SRON [66], the Dutch Ministries of Research and Education and Economic Affairs as well the Technology Foundation STW, Applied Science Division of NWO for funding the research. We also wish to thank A.F. Meunier and G.M. Thubé (École polytechnique de l'université d'Orléans, France) for their contributions to the experimental results.

## 8.9 2D images of the metal-halide lamp obtained by experiment and model

**Abstract.**
The metal-halide lamp shows colour segregation caused by diffusion and convection. Two-dimensional imaging of the arc discharge under varying gravity conditions aids in the understanding of the flow phenomena. We show results obtained by experiments and by numerical simulations in PLASIMO.

The metal-halide (MH) lamp is a compact high-intensity light source with a high luminous efficacy and a good colour rendering index [3]. The arc discharge lamp contains a buffer gas (Hg) and metal additives (for instance Na, Ce, Dy) dosed as metal-halide salts. These metal additives improve the colour rendering. The additive density distribution is determined by convective and diffusive processes (due to the high radial temperature gradient). When these processes are in the same order of magnitude, the competition between them leads to axial segregation of the metal additive, then segregation of colours appears (figure 8.16(a)) [27, 28, 32, 33, 38]. Because the convection is induced by gravity, a centrifuge that can go up to $10g$ was built to vary the amount of convection (chapter 4) [37].

We can look at the plasma of the MH lamp in different ways. Two-dimensional imaging of the plasma in the MH lamp gives insight into the flow phenomena and hence the segregation inside the lamp. Here, we investigate one particular MH lamp at different gravity conditions and present colour pictures taken by an ordinary webcam and 2D metal additive density profiles measured by Imaging Laser Absorption Spectroscopy (ILAS; section 4.3.2) [37]. Besides these experimental results we show several images representing physical quantities in the lamp, obtained by numerical simulations in PLASIMO [70, 86].

The MH lamp is a COST reference lamp (section 1.3.1) [27] and contains 10 mg Hg as buffer gas, 300 mbar $Ar/Kr^{85}$ as starting gas and 4 mg $DyI_3$ as salt additive. The diameter of the lamp burner is 8 mm and the burner height is 20 mm (electrode distance 16 mm). The input power is 148.4 W.

Figure 8.16 shows a picture of the lamp taken by a digital camera and webcam images taken from $1g$ to $10g$. The directly visible colour segregation is clearly seen at $1g$. The bluish-white light at the bottom originates from Dy atoms. Towards the top the colour is bluish-greenish, which is due to Hg atoms. At higher gravity one sees that the axial colour segregation is diminished: the Dy atoms are more evenly distributed over the lamp, caused by the increased amount of convection.

The line-of-sight ground state atomic Dy density is obtained by ILAS. With ILAS, a laser beam is expanded so that it illuminates the whole lamp burner. A part of the laser light is absorbed by the Dy atoms. After passing the lamp burner the remaining laser light hits a CCD camera. From this remaining intensity, the absorption and hence the

density is calculated at each position in the lamp burner; this gives an indirect image as nonradiative particles are measured. In figure 8.17, the same effect is seen as at the webcam images. At normal gravity ($1g$), the Dy atoms stay mainly at the bottom of the plasma; the maximum is found somewhere between the centre and the wall of the plasma. When gravity is increased, the maximum of the atomic Dy density moves upward and at the same time the Dy atoms are more evenly distributed over the lamp.

In addition to the direct and indirect images of the plasma obtained by experiments, the lamp has been studied by numerical simulations in PLASIMO [70, 86]. This model assumes local thermodynamical equilibrium. The temperature is calculated from the energy balance, whereas the bulk flow follows from the Navier Stokes equation. Figure 8.18 shows the ground state atomic Dy density, the temperature distribution, the axial convection speed and the electron density; all at $1g$ and $2g$. The Dy densities are line-of-sight integrated densities (lateral position on horizontal axis), whereas the other images are radial densities (radial position on horizontal axis). When one compares figure 8.18(a) and (b) with the experimental results in figure 8.17(a) and (b), the same trend is observed: the shape of the Dy density is in agreement and it is seen that at higher gravity the Dy atoms are more evenly distributed over the lamp. Figures 8.18(c) and (d) show the strong radial gradient in temperature. The axial convection speed is shown in figure 8.18(e) and (f); positive values correspond to an upward flow whereas negative values correspond to a downward flow. The convection speed increases linearly with gravity; the figures show that the convection speed at $2g$ is twice as high as at $1g$. Finally figure 8.18(g) and (h) show the electron density distribution over the lamp burner.

In conclusion, the MH lamp can be investigated by different methods, which gives 2D images of the plasma in different ways. The colour segregation that is observed at the webcam images at different gravity is directly correlated to the Dy density images obtained by ILAS. Modelling of the same lamp also offers Dy density images, which are in agreement with the experimental results, and other physical quantities.

The authors are grateful to A.F. Meunier and G.M. Thubé, Philips ADL, SenterNovem (project EDI 03146), SRON and the Dutch Ministries of Research and Education as well as Economic Affairs for funding the research.

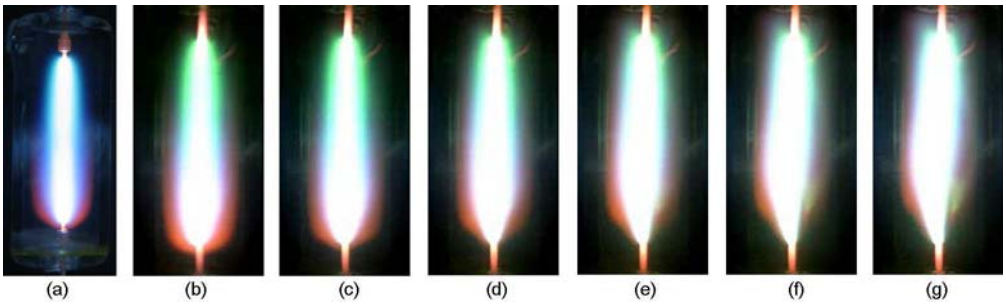


**Figure 8.16:** (a) Picture of the lamp at $1g$; (b)–(g) webcam images at $1g$, $2g$, $4g$, $6g$, $8g$, $10g$.

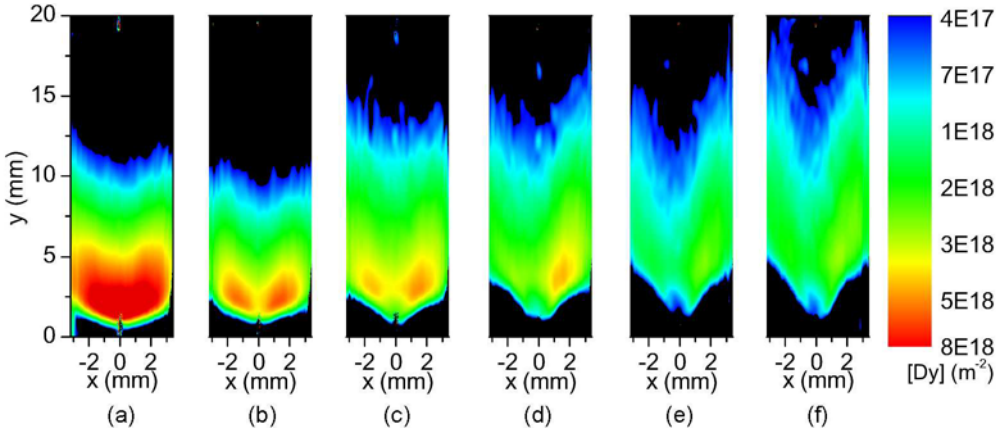


**Figure 8.17:** Imaging Laser Absorption Spectroscopy (ILAS) images at $1g$, $2g$, $4g$, $6g$, $8g$, $10g$.

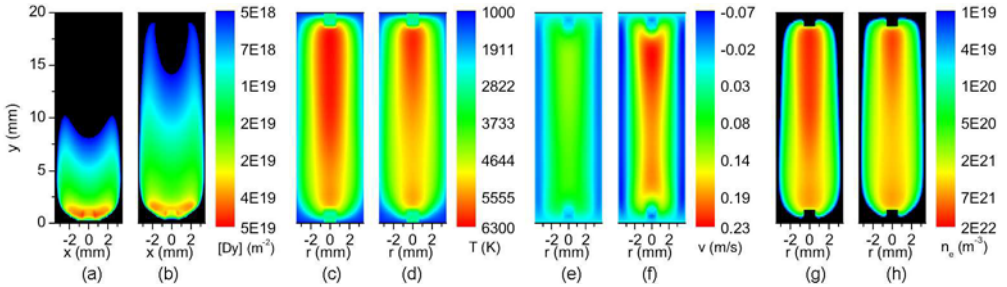


**Figure 8.18:** Simulations (PLASIMO) at $1g$ and $2g$: (a)–(b) ground state Dy density; (c)–(d) temperature; (e)–(f) axial convection speed; (g)–(h) electron density.